J Low Temp Phys (2014) 175:590–603
DOI 10.1007/s10909-014-1095-7

Contribution of Chirality to the Adsorption of a Kr Atom on a Single Wall Carbon Nanotube

Hye-Young Kim · Eric C. Booth · Mamadou T. Mbaye · Silvina M. Gatica

Received: 28 October 2013 / Accepted: 16 January 2014 / Published online: 6 February 2014

Abstract Recent theoretical and simulation studies (Lueking et al. Phys Rev B 75:195425, 2007; Kim et al. J Phys Chem 115:7249–7257, 2011) on the adsorption of Kr on suspended nanotubes yielded different commensurate phases at submonolayer coverage than those found in a pioneering experiment (Wang et al. Science 327:552–555, 2010). This controversy between calculations and experiments is yet to be resolved. One of the tentative explanations of the apparent discrepancy is the possibly different chirality as the chirality of the nanotubes used in the experiment is not known. To address the question on chirality, we calculated the adsorption potential of krypton atoms on two sets of single wall carbon nanotubes of same radii with distinct chiralities. We found novel symmetries of the adsorption sites on a nanotube, which systematically vary depending on its chirality with an unexpected, yet intuitive delicacy. The same approach is equally feasible for other gases (Ar, Xe, CH_4, etc.). The results of classical grand canonical Monte Carlo simulations confirm the predicted behavior of adsorption phases.

Keywords Single wall carbon nanotube · Chirality · Krypton adsorption phase · Adsorption potential · Surface corrugation · Grand Canonical Monte Carlo

1 Introduction

A series of pioneering experiments were conducted by the group of Cobden and Vilches [1,2], involving gas adsorption on a suspended single wall carbon nanotube

H.-Y. Kim (✉) · E. C. Booth
Department of Chemistry and Physics, Southeastern Louisiana University, Hammond, LA 70402, USA
e-mail: hye-young.kim@selu.edu

M. T. Mbaye · S. M. Gatica
Department of Physics and Astronomy, Howard University, Washington, DC 20059, USA

(CNT). They measured the mass adsorption isotherm using a resonant frequency technique, qualitatively similar to that employed in the quartz crystal microbalance [3,4]. Specifically, to our current interest, they found that Kr forms a submonolayer phase of fractional coverage $\varphi = 1/6$, which they assume it corresponds to the $\sqrt{3} \times \sqrt{3}$ R30° commensurate solid (CS). Here, the dimensionless parameter φ is defined as the number of adsorbed atoms per carbon atom.

Kr is known to form a $\sqrt{3} \times \sqrt{3}$ R30° CS phase at low temperature on top of flat graphite [5]. As the CNT is notionally a rolled-up graphene, similar CS phases have been expected to develop on the surface of a CNT. Those phases were predicted by ground-state energy calculations [6] and reportedly observed by Cobden-Vilches experiments [1,2]. A later study of grand canonical Monte Carlo (GCMC) simulations [7], however, exhibited an apparently significant disagreement for Kr; Kr forms a submonolayer CS phase of $\varphi = 1/4$ for zigzag (18,0) and an IS phase of $\varphi = 1/4$ for armchair (12,12) nanotubes of diameters D = 1.41 nm and 1.63 nm, respectively. As the Cobden-Vilches group estimated their nanotube diameters to be in the range of 1–3 nm, this apparent controversy still is an open question. To resolve this discrepancy, the precise measurement of the nanotube radius and chirality is critical.

On the other hand, we note here that the computational and theoretical studies are not free from their own flaws. Physical adsorption of simple atoms or molecules on CNT has been studied extensively due to their many environmental, industrial, and medical applications [8–13]. To be able to interpret experimental data properly or to make accurate predictions from theoretical calculations or computer simulations, one needs accurate potential models. However, our understanding of the gas-surface adsorption potential V(r) of CNTs is not complete. More advanced experimental, theoretical and simulation studies are needed for corresponding comparisons to develop a better model of V(r) on nanotubes, and the present work is in that vein.

In this paper we calculate the surface corrugation using the commonly adopted pairwise adsorption potentials, to demonstrate how thereby obtained corrugation symmetries depend on the chirality and differ from that of planar graphite or graphene. The results of the present calculations, specifically the microscopic layout (or map) of the chirality-dependent surface corrugation symmetry, can be tested in the future not only against the experimental observations but also against the full quantum calculations, to obtain a better force field for the gas adsorption potential on CNTs. The results of our calculation reveal novel symmetries of the adsorption sites on a nanotube, depending on its chirality. These results are consistent with the analysis based on the broken symmetry of CNTs relative to that of planar graphite [14]. Also, the adsorption phase trend predicted based on the chirality dependence found in the present study is confirmed by GCMC simulations results. Even though we focus on Kr on CNT in this work, the same approach is perfectly feasible for other gases (Ar, Xe, CH_4, etc.) some of which are being studied by the Cobden-Vilches group.

In this paper, we report the novel contribution of chirality to the adsorption potential of a CNT. Section 2 introduces the adsorption potential formulations and parameters used in the calculations and Section 3 presents the results of our calculations, which demonstrate the varying symmetry in the adsorption surface of nanotubes due to the different chirality. Section 4 describes the results of our simulations confirming the behavior predicted in Section 3. Finally, we present the conclusions in Section 5.

2 Adsorption Potentials

The adsorption potential is defined as the difference between the electronic ground state energy of the system of an atom and a substrate, at finite separation, and its value at infinite separation. In principle one may solve the Schrödinger equation or an equivalent density functional equation to get the electronic density. However, there are difficulties with this approach, arising mainly from the fact that it is a many-body problem involving a large number of electrons. The conventional way to deal with this problem, in a system involving many atoms, is to assume that the adsorption interaction, V(r), arises from the addition of the short-range repulsion due to the overlap of electronic densities and the long-range attraction due to van der Waals interactions. As more advanced experimental and simulation studies are being conducted, a better knowledge of V(r) is in great need in order to understand the experimental observations or make accurate predictions.

Most current experimental and simulation studies adopt V(r) as a sum of semiempirical pair interactions $U_2(\mathbf{x})$ between the adsorbed atom (henceforth called adatom) at $\mathbf{r}_a$ and individual Carbon (C) atoms:

$$V(\vec{r}_a) = \sum_i U_2(\vec{r}_a - \vec{r}_{C_i}) = \sum_i U_2(\vec{x}_i). \tag{1}$$

Here the sum is over all C atom sites ($\mathbf{r}_{Ci}$), and x_i is the separation between the adatom and the i-th C atom. There are two commonly used semiempirical forms of $U_2(x)$: (a) the simplest *isotropic* Lennard-Jones (LJ) 12-6 potential and (b) the *anisotropic* pair potential function adapted to include the anisotropy of the C atoms on graphite which originates in the anisotropic π-bonds [15–17]. The more advanced form of the anisotropic pair potential function is [15,16]:

$$\begin{aligned} &U_2^{aniso}(x) \\ &= 4\varepsilon_{aC}\left[(\sigma_{aC}/x)^{12}\{1+\gamma_R\left[1-(6/5)\cos^2\theta\right]\} - (\sigma_{aC}/x)^6\right. \\ &\quad \left.\{1+\gamma_A\left[1-(3/2)\cos^2\theta\right]\}\right]. \end{aligned} \tag{2}$$

Here θ is the angle between the interatomic separation vector $\mathbf{x} = \mathbf{r}_a - \mathbf{r}_{Ci}$ and the radial vector, normal to the nanotubes's surface at the C-atom position $\mathbf{r}_{Ci}$. The values commonly used for a system of Krypton atoms on CNT are $\gamma_R = -0.54$ [18,19], $\gamma_A = 0.37$ [18,19], $\sigma_{aC} = 0.36$ nm [20,21], and $\varepsilon_{aC} = 69.2$ K [20,21]. This functional form and parameters are proven to be accurate for simple gas systems on graphite [5]. When one lets the anisotropy parameters $\gamma_R = \gamma_A = 0$, Eq. (2) returns the isotropic LJ 12-6 potential, the simplest form of the pair-wise potential:

$$U_2^{iso}(x) = 4\varepsilon_{aC}\left[(\sigma_{aC}/x)^{12} - (\sigma_{aC}/x)^6\right]. \tag{3}$$

The attractive second term in Eq. (2) is the anisotropic 2-body van der Waals interaction and the value of γ_A is given by [22]:

$$\gamma_A = -(2/3)(1-b)/(1+b), \tag{4}$$

$$b = \frac{\alpha_{C\perp}}{\alpha_{C//}} \frac{(1+E_a/E_{C//})}{(1+E_a/E_{C\perp})} \cong \frac{\alpha_{C\perp}}{\alpha_{C//}}. \tag{5}$$

The subscripts // and $\perp$ refer to directions parallel and perpendicular, respectively, to the surface normal, i.e., the radial direction of the CNT. The quantities Ea, $E_{C//}$ and $E_{C\perp}$ are characteristic energies of adatoms and C atoms, which are typically chosen as the atomic ionization energies within the single-excitation energy approximation commonly employed in the Drude atomic model [5]. The right-most term in Eq. (5) is from the common assumption that $E_{C//} \approx E_{C\perp}$ [15,16]. In the study of both He/graphite [15,16] and He/graphene [23], the anisotropy ratio of C-atom b = 3.5 is determined based on the dielectric data [18,19,24] and found that the inclusion of anisotropy in the pair wise interaction increases the surface corrugation. This model of the anisotropic potential has been widely used in many studies of simple gases adsorbed on graphite, graphene, and nanotubes. However, it is not clear if this value of b, being estimated from planar graphite, should remain the same for C-atoms composing a CNT. In recent years, there have been a number of studies on the polarizability of CNTs [25–28]. While most of these studies were interested in estimating the polarizability of a cabon nanotube itself, Langlet et.al. [25] reported the values of the anisotropic "atomic" polarizability of C atoms on a CNT which have been fitted in order to recover the measured polarizability of C_{60} and C_{70} [27] as well as the results of the tight-binding calculation for the CNT polarizability [27]. These values of the anisotropic polarizability of the C atom are $\alpha_{C\perp} = 2.47 \times 10^{-3}\text{nm}^3$ and $\alpha_{C//} = 8.7 \times 10^{-4}\text{nm}^3$, from which we obtain the anisotropy ratio b = 2.906 (γ_A = 0.325). To the best of our knowledge, there have been no further studies for simple gas atoms/molecules on CNT using these parameters. For these reasons, we evaluated the adsorption potential using anisotropic pair potentials in Eq. (2) adopting both values of b, 3.5 and 2.906. The results, however, exhibit the same *qualitative* conclusions on the chirality dependence of V(r), which is our main interest. Therefore, only the results using b = 3.5 (γ_A = 0.37) are presented henceforth.

3 Chirality-Dependence in the Surface Corrugation of a CNT

Planar graphene, assuming an infinitely large size so we may ignore the edge effect [29,30], has two-dimensional translational lattice symmetry identical to that of the graphite basal plane. As an atom approaches the surface of graphene, there are three distinct adsorption sites; above a carbon atom (A), above a hexagonal site (S), and above a saddle-point between two carbon atoms (SP) (see Fig. 1a). Each hexagon in the honeycomb pattern has one S, six equivalent A, and six equivalent SP sites. S and A are the most- and the least-favored adsorption sites, respectively, and the difference of the adsorption potential between these two represents the surface corrugation [31,32].

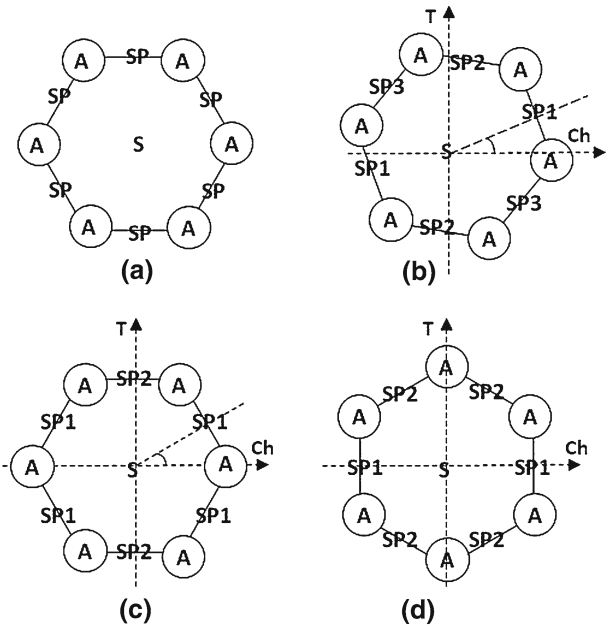

Fig. 1 Adsorption sites on **a** a planar graphene, **b** a chiral tube with chiral angle ϕ, **c** an armchair tube with chiral angle $\phi = 30°$, and **d** a zigzag tube with chiral angle $\phi = 0°$. For a planar graphite basal plane or a graphene, all SP-sites are equivalent and are denoted as SP. For a nanotube, each distinct SP-site is numbered (SP1, SP2, and then SP3 for a chiral tube, for example) in the order it appears as the angle from the chiral axis increases in the counter-clock-wise direction

However, as a graphene sheet notionally rolls up to construct a cylindrically shaped nanotube with a certain chiral angle, a three-dimensional molecular symmetry should be considered [33]. As a result, not all six SP sites in a hexagon share the same symmetry any more, while all S and A sites on the nanotube remain equivalent. For example, there are three distinct SP sites (two SP1, two SP2 and two SP3 in a hexagon) in a chiral tube in general as shown in Fig. 1b. These three distinct SP-sites are numbered (SP1, SP2, and then SP3) in the order they appear as the angle from the chiral axis increases in the counter-clock-wise direction. For zigzag and armchair tubes, there are only two distinct SP sites due to the symmetry: four SP1 and two SP2 sites in a hexagon for an armchair and two SP1 and four SP2 sites in a hexagon for a zigzag CNT as shown in Fig. 1c, d.

To assess solely the contribution of chirality on V(r), separated from the contribution of curvature or radius, we have selected two subsets of three tubes {(12,0); (11,2); (7,7)} and {(21,0), (15,9), (12,12)}. These three CNTs in each set have distinctly different chiral angles, yet have diameters (0.94 and 1.64 nm, respectively) that are identical within a margin of a couple of hundredths of a nanometer. The chiral nanotubes (11,2) and (15,9) provide an intermediate chiral angle (8.2° and 21.8°, respectively) between those of the zigzag (0°) and armchair (30°) nanotubes. We note here that, regardless of b values (or the anisotropy of carbon atoms), no difference was found between right-handed and left-handed chiral nanotubes in our calculations,

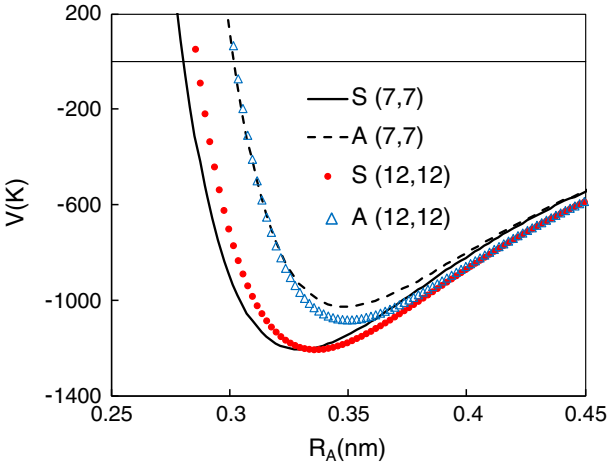

Fig. 2 Adsorption potentials at S sites (*solid curve* and *dots*) and A sites (*broken curve* and *open triangles*) for a Kr atom on armchair (7,7) and (12,12) nanotubes. The potentials of S and A sites, independently, for all three chiralities of same radius overlap within the resolution of this graph. R_A is the elevated radial distance of the Kr atom above the carbon atoms on the nanotube (Color figure online)

which agrees with the findings reported in Ref. [34]. Therefore, only the results of the right-handed chiral nanotubes will be presented henceforth.

The adsorption potentials of S and A sites are plotted in Fig. 2 as a function of the radial distance (R_A) of the Kr atom above the nanotube surface. Note that the adsorption potential curves for all S and A sites on three nanotubes of different chirality in each subset are indistinguishable within the resolution of the plot. This demonstrates that V(r) and the corrugation (traditionally measured as the difference of V(r) at S and A sites) are mainly determined by the radius of CNT, not the chirality [7,35]. Figure 2 shows that the corrugation decreases as the radius increases or as the curvature decreases as expected. On the other hand, small but appreciable differences in the well depth of V(r) are observed for various SP sites on each nanotube of varying chirality as shown in Figs. 3–5. A closer inspection shows that these differences of adsorption potential demonstrate a systematic dependence on the chiral angles, and thus the signature pattern of surface corrugation for a tube of a given chiral angle (see Fig. 6).

To assess the "preference" of a Kr atom towards a given adsorption site, the potential difference $\Delta V(r)$ defined as the difference between the adsorption potential of a non-A-site and an A-site is calculated as a function of the radial distance (R_A) of the Kr atom above the tube surface (see Figs. 3–5). A positive $\Delta V(r)$ represents an energetically less favored region than site A. For planar graphite/graphene, $\Delta V(r)$ would be negative at all SP and S sites. The values of $\Delta V(r)$ for all CNTs of varying radius and chirality we have studied reveal that S is consistently the most favored adsorption site, a result that agrees with the graphene/graphite case. Also, both SP2 and SP3 remain favored over A-site independent of the chirality, which again agrees with graphene/graphite case. On the other hand, SP1 site remains consistently the least favored regardless of the chirality within the first monolayer adsorption range of $0.25 < R_A < 0.55$ nm we

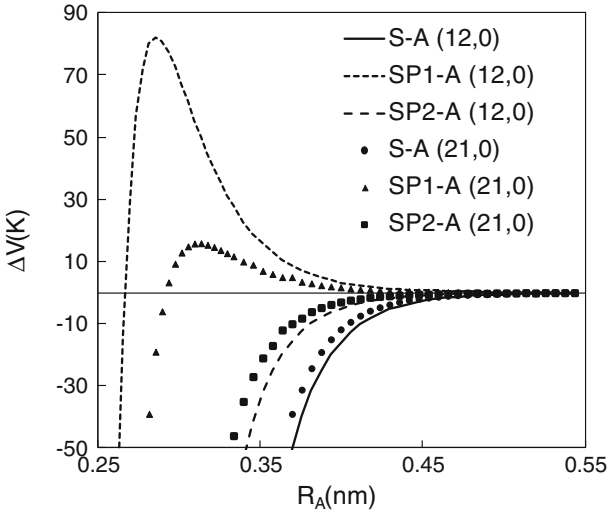

Fig. 3 The potential difference $\Delta V(r)$ of adsorption potential at sites [S, SP1 and SP2] to that at site A as defined in the text for two zigzag nanotubes of different radius. The *curves without* and *with symbols* represent the $\Delta V(r)$ for CNTs (12,0) and (21,0), respectively. Note that positive $\Delta V(r)$ corresponds to the region which is energetically less favored than site A. Here, SP1 becomes less favored than the A site at R_A = 0.267 and 0.291 nm, respectively for CNTs (12,0) and (21,0), and remains unfavorable for greater R_A

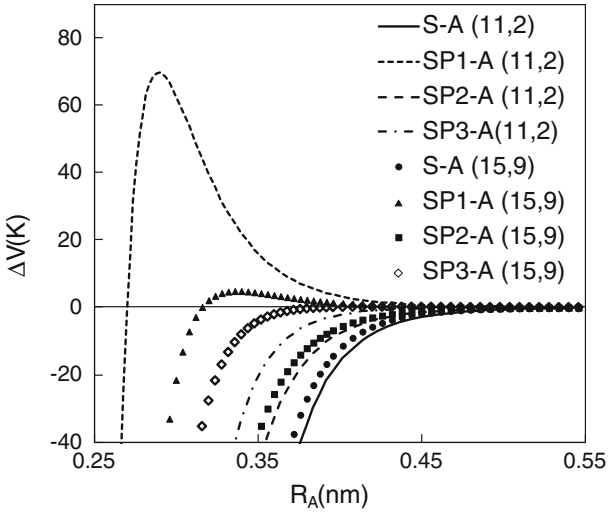

Fig. 4 The potential difference $\Delta V(r)$ of adsorption potential at sites [S, SP1, SP2, and SP3] to that at site A as defined in the text for two chiral nanotubes of different radius. The *curves without* and *with symbols* represent the potential difference $\Delta V(r)$ for CNTs (11,2) and (15,9), respectively. Note that positive $\Delta V(r)$ corresponds to the region which is energetically less favored than site A. Here, SP1 becomes less favored than the A site at R_A = 0.270 and 0.313 nm, respectively for CNTs (11,2) and (15,9), and remains unfavorable for greater R_A

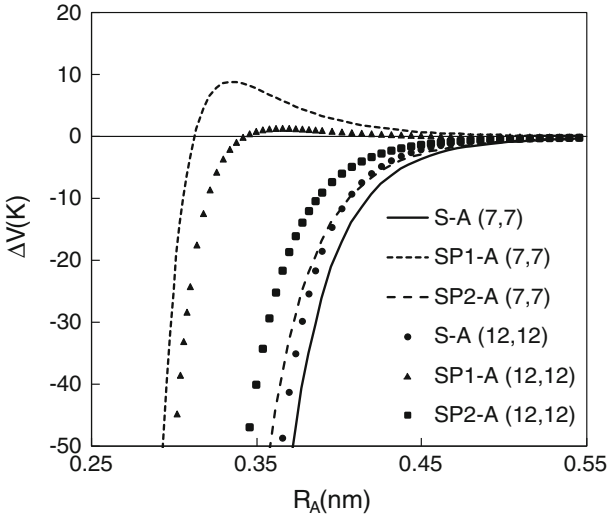

Fig. 5 The potential difference $\Delta V(r)$ of adsorption potential at sites [S, SP1, and SP2] to that at site A as defined in the text for two armchair nanotubes of different radius. The *curves without* and *with symbols* represent the potential difference $\Delta V(r)$ for CNTs (7,7) and (12,12), respectively. Note that positive $\Delta V(r)$ corresponds to the region which is energetically less favored than site A. Here, SP1 becomes less favored than the A site at $R_A = 0.312$ and 0.342 nm, respectively for CNTs (7,7) and (12,12), and remains unfavorable for greater R_A

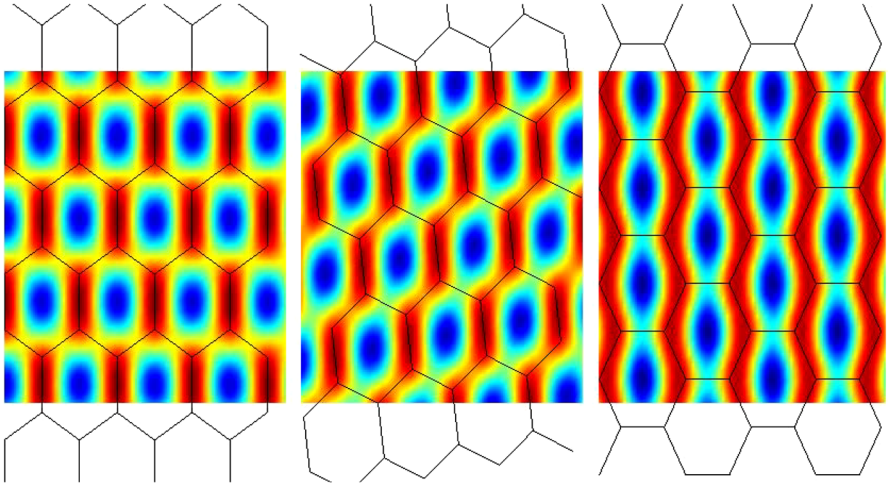

Fig. 6 Contour plot of the adsorption potential of a Krypton atom on a single wall nanotube: zigzag (12,0), chiral (11,2) and armchair (7,7) from *left* to *right*. The radial distance (R_A) above the CNT is 0.35 nm. The contour plot is colored in *blue* (the most attractive adsorption sites), *green*, *yellow* and *red* (the least attractive adsorption sites) in the order of the strength of the adsorption potential (Color figure online)

have explored. This simple and intuitive, yet unpredicted, result has not been discussed elsewhere to the best of our knowledge.

Specifically, in the smaller radius CNT subset, SP1 becomes less favored than the A site at R_A equal to and larger than 0.267, 0.270, and 0.312 nm, respectively, for

zigzag (12,0), chiral (11,2), and armchair (7,7) tubes. Similarly, in the larger radius subset, SP1 becomes unfavored over A site at the range of R_A: 0.291, 0.313, and 0.342 nm, respectively, for zigzag (21,0), chiral (15,9), and armchair (12,12) tubes. The corrugation on a planar graphite/graphene substrate is traditionally measured as the difference between the most favored (S) and the least favored (A) sites. Following this conventional definition of surface corrugation and based on our findings, we conclude that the corrugation of a CNT should be measured as the difference between the most attractive (S) and the least attractive (SP1) sites. Note that the difference between the S and A sites remains intact regardless of its chirality and the level of "disfavorability" of the SP1 sites over A sites decreases as the chiral angle increases. Since the armchair tube exposes the smoothest surface with the least $\Delta V(r)$ to adsorbed atoms than CNTs of other chiral angle, including zigzag tubes, the armchair nanotube is expected to have a greater tendency to form an incommensurate ordered phase. This expectation is confirmed by the results of the grand canonical Monte Carlo (GCMC) simulations described in the next section and in our previous study [7], which find commensurate and incommensurate ordered phases for Kr monolayer on zigzag and armchair CNTs, respectively. This novel change in the adsorption environment, due to the different symmetry in the surface corrugation on a given chiral nanotube, stands in marked contrast to the planar graphene/graphite case.

4 Grand Canonical Monte Carlo Simulations of Krypton Adsorbed on Armchair and Zigzag CNTs.

The results described in the previous section show that the surface corrugation changes systematically with the chirality. It is expected, therefore, that a zigzag nanotube would offer a more favorable environment for a CS phase than an armchair nanotube of the same radius.

As we mentioned before, in our previous study [7] we found a CS phase in a zigzag (18,0) nanotube, and no evidence of any such a phase in an armchair (12,12) nanotube. Here we extend the study to pairs of armchair and zigzag nanotubes of equal radius. For this sake, we have run a series of Grand Canonical Monte Carlo simulations for Krypton adsorbed on two pairs of CNTs with diameter from 1.64 and 2.58 nm. Our method of simulation is described in Ref. [7]. The potential interaction between the Kr atoms and the carbon atoms is given in Eq. (3), with parameters $\gamma_R = -0.54$ and $\gamma_A = 0.37$. All the simulations were done at a temperature of 77.4 K.

We inspect the results of our simulations searching for features that may indicate the occurrence of a CS phase. These features are steps in the energy isotherms: a step down in the energy gas-surface usually indicates a transition to a commensurate state. Once the features are identified, we confirm the phase by inspecting the structure of the adsorbate. We calculate two functions to test the structure: the two-dimensional radial distribution function (RDF) and the structure function. The RDF is defined as

$$g(r) = N_r/(2\pi\ r\ dr\Theta) \tag{6}$$

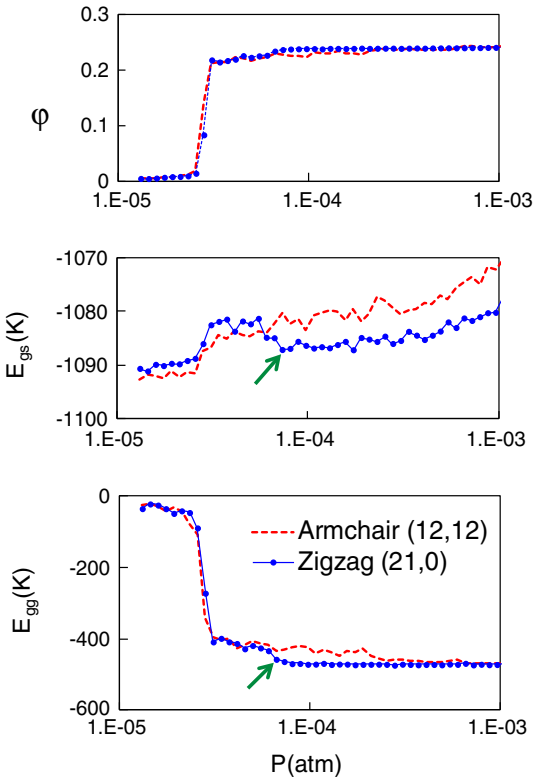

Fig. 7 Partial coverage φ (*top*), E_{gs} (*middle*) and E_{gg} (*bottom*) as a function of the pressure of the vapor for Kr adsorbed in CNTs (12,12) and (21,0) as indicated in the legend. The temperature is 77.4 K. The *arrows* indicate the formation of the CS phase (Color figure online)

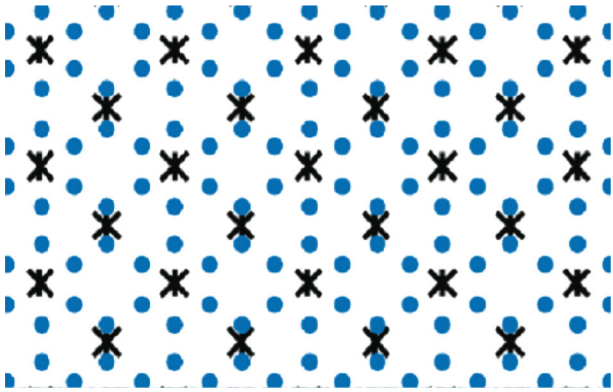

Fig. 8 Schematic view of the 1:4 CS phase (adapted from Ref. [7]). *Light blue circles* represent C atoms while the *asterisks* represent Kr atoms (Color figure online)

where N_r is the number of atom-pairs at a distance between r and r + dr in the unrolled plane, and Θ is the number of atoms per unit area. We refer the reader to Ref. [7] for the description of the structure function, basically the Fourier transform of the pair correlation function. The results of our simulations are displayed in Figs. 7–10.

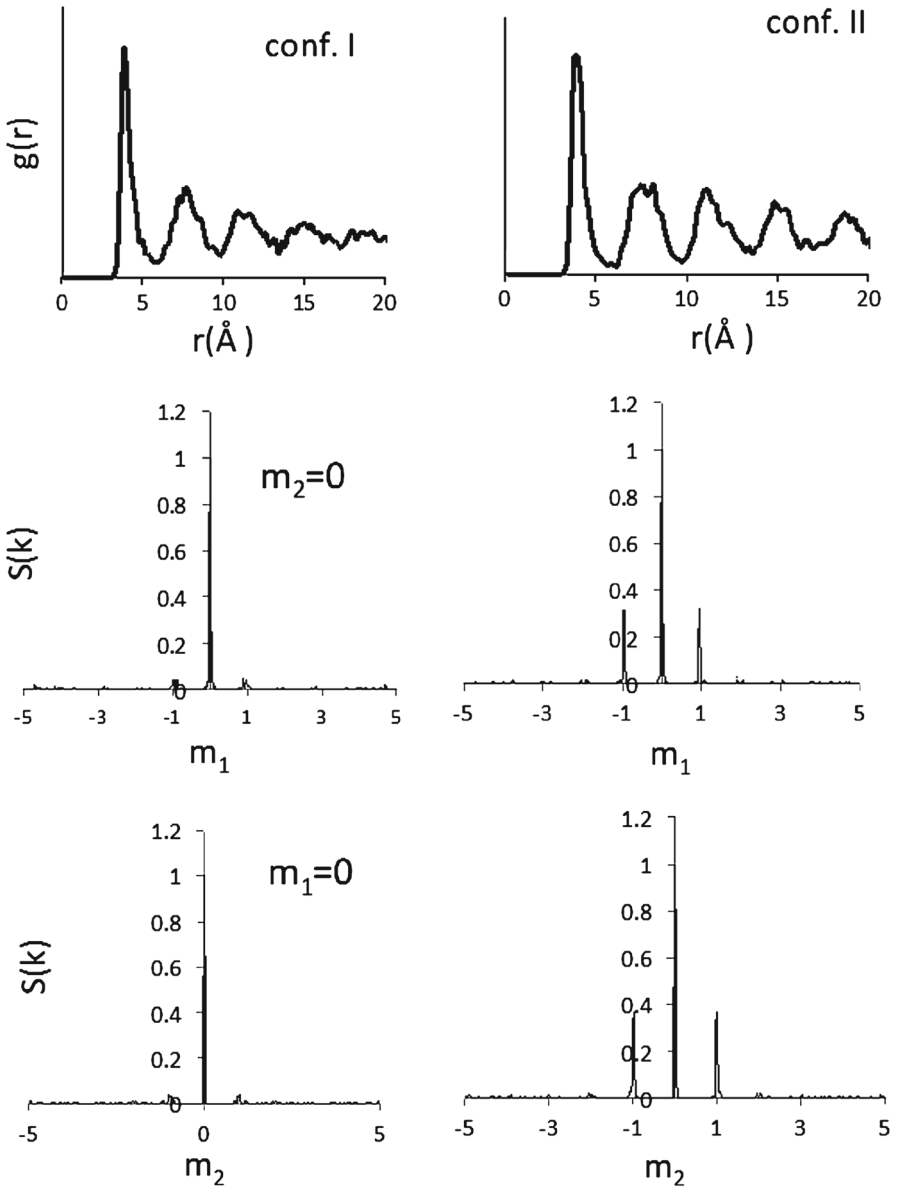

Fig. 9 Two-dimensional radial distribution function (*first row*); structure function as a function of variable m_1 for the case $m_2 = 0$ (*second row*) and as a function of m_2 for $m_1 = 0$ (*third row*). The *left* (*right*) column corresponds to configuration I (II)

In Fig. 7, we plot the fractional coverage (φ), defined as the number of Kr atoms adsorbed per carbon, the gas-surface energy per particle (E_{gs}) and the gas-gas energy per particle (E_{gg}) as functions of the vapor pressure, for the pair of CNTs armchair (12,12) and zigzag (21,0) (both with diameter 1.64 nm). We recognize the first step

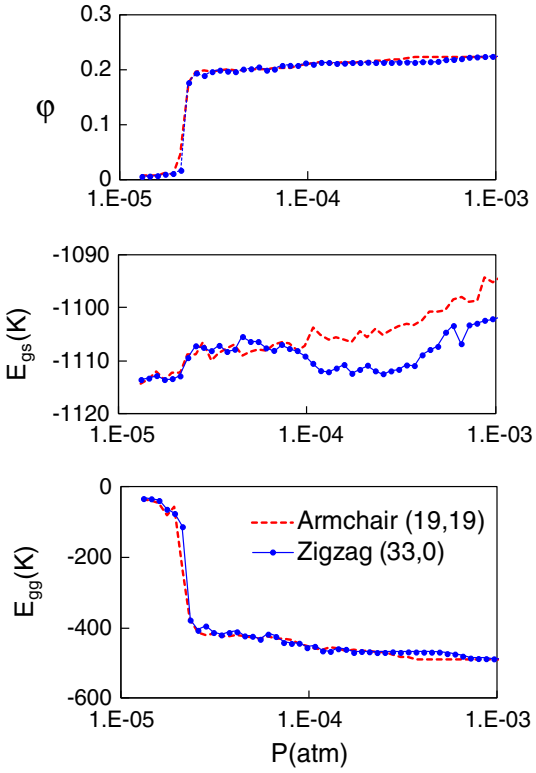

Fig. 10 Partial coverage φ (*top*), E_{gs} (*middle*) and E_{gg} (*bottom*) as a function of the pressure of the vapor for Kr adsorbed in CNTs (19,19) and (33,0) as indicated in the legend. The temperature is 77.4 K (Color figure online)

in the coverage that corresponds to the condensation of a monolayer, at a pressure $P_u = 2.56 \times 10^{-5}$ atm, for both the armchair and zigzag CNTs. We call this pressure "uptake pressure", P_u. The transition is accompanied by a decrease in the E_{gg} and an increase in E_{gs}, a consequence of a rise in the density of the adsorbate. We note that the value of P_u is independent of the chirality of the CNTs. At a higher pressure $P_c = 7.0 \times 10^{-5}$ atm, we observe a step down in Egs *only* for the zigzag CNT, indicating the formation of a commensurate phase. We notice that, at the same pressure, the E_{gg} decreases by 38 K; hence the phase formed favors both the gas-surface and gas-gas interactions. The fractional coverage of this CS phase is $\phi = 0.24$, close to the value observed in Ref. [7] ($\varphi = 1/4$).

We confirm the commensuration by inspecting the RDF and the structure function for two sample configurations at pressures below and above P_c. For the calculation of $s(\mathbf{k})$ we assume $\mathbf{k} = m_1\mathbf{b}_1 + m_2\mathbf{b}_2$, where (m_1, m_2) are integer numbers and $(\mathbf{b}_1, \mathbf{b}_2)$ are the reciprocal lattice vectors corresponding to the 1:4 CS phase found in Ref. [7]. This lattice is made of S and SP sites as schematically shown in Fig. 8.

In Fig. 9, we plot the RDF and the structure function of two configurations, I and II. The first configuration correspond to $P = 5.5 \times 10^{-5}$ atm (below P_c) with $E_{gs} = -1081.3$ K. The second one corresponds to $P = 7.3 \times 10^{-5}$ atm (above P_c) and $E_{gs} = -1087.1$K. We observe that the structure function of configuration II presents

pronounced peaks, opposite to that of configuration I, confirming that II is a CS phase. Comparing the RDF of I and II we notice that configuration I seems closer to a liquid phase than II. For the armchair CNT (12,12), there is no indication of a CS phase since the E_{gs} increases monotonically. The E_{gg}, on the other hand, steps down by 42 K at a higher pressure than the zigzag counterpart. We believe that this indicates the formation of an incommensurate solid phase.

The results for the armchair (19,19) and zigzag (33,0) CNTs, both with diameter 2.58 nm are shown in Fig. 10. The behavior is qualitatively the same as for the 1.64 nm-pair: Kr forms a CS phase in the zigzag tube *only* at $P_c = 1.2 \times 10^{-4}$ atm with a gas-surface energy decrease of 4K.

5 Conclusions

We have analyzed and discussed how the adsorption potential, and thus the surface corrugation, varies based on the chirality of nanotubes. We find that the surface corrugation changes in a systematic way as chirality changes. The change occurs not just in magnitude but in symmetry as well. In terms of magnitude, the adsorption surface becomes smoother as the chiral angle increases. In terms of symmetry, there are different shapes and areas of favored regions (or channels) on a nanotube depending on the chirality as can be seen clearly in Fig. 6. This induces a novel adsorption environment with varying surface corrugation for the adatoms on each CNT of different chirality. The predictions based on the surface corrugation are confirmed by our GCMC simulations. In conclusion, the behavior of ordered or disordered phases of atoms and molecules adsorbed on CNTs is found to depend strongly on the chirality, and thereby is quite different from that of these phases on graphene/graphite.

Acknowledgments Kim acknowledges the support from Louisiana Board of Regents-RCS Grant (LEQSF(2012-15)-RD-A-19). Mbaye and Gatica acknowledge the support from NSF (DMR 1006010). Kim thanks Milton Cole for helpful comments on the earlier version of the manuscript.

References

1. Z. Wang, J. Wei, P. Morse, J.G. Dash, O.E. Vilches, D.H. Cobden, Science **327**, 552–555 (2010)
2. H.-C. Lee, O.E. Vilches, Z. Wang, E. Fredrickson, P. Morse, R. Roy, B. Dzyubenko, D.H. Cobden, J. Low Temp. Phys. (2013). doi:10.1007/s10909-012-0642-3
3. T. Coffey, J. Krim, Phys. Rev. Lett. **95**, 076101 (2005)
4. J. Krim, A. Widom, Phys. Rev. B **38**, 12184–12189 (1988)
5. L.W. Bruch, M.W. Cole, E. Zaremba, *Physical adsorption: forces and phenomena*, vol. 6 (Dover Publications, Mineola, 2007)
6. A.D. Lueking, M.W. Cole, Phys. Rev. B **75**, 195425 (2007)
7. H.-Y. Kim, M.W. Cole, M. Mbaye, S.M. Gatica, J. Phys. Chem. **115**, 7249–7257 (2011)
8. J. Watson, K. Ihokura, MRS Bull. **24**, 14–15 (1999)
9. J.H. Seinfeld, S.N. Pandis, *Atmospheric chemistry and physics: from air pollution to climate change* (Wiley, New York, 1998)
10. M.P. Anantram, F. Leonard, Rep. Prog. Phys. **69**, 507–561 (2006). and references therein
11. Y. Takao, K. Miyazaki, Y. Shimizu, M. Egashira, J. Electrochem. Soc. **141**, 1028–1034 (1994)
12. R.H. Baughman, A.A. Zakhidov, W.A. de Heer, Science **297**, 787–792 (2002)
13. P. Cherukuri, C.J. Gannon, T.K. Leeuw, H.K. Schmidt, R.E. Smalley, S.A. Curley, R.B. Weisman, Proc. Natl. Acad. Sci. USA **103**, 18882–18886 (2006)

14. G.G. Samsonidze, R. Saito, A. Jorio, M.A. Pimenta, A.G. Souza Filho, A. Grüneis, G. Dresselhaus, M.S. Dresselhaus, J. Nanosci. Nanotech. **3**, 431–458 (2003)
15. W.E. Carlos, M.W. Cole, Phys. Rev. Lett. **43**, 697–700 (1979)
16. W.E. Carlos, M.W. Cole, Surf. Sci. **91**, 339–357 (1980)
17. L.W. Bruch, H. Watanabe, Surf. Sci. **65**, 619–632 (1977)
18. W.E. Carlos, M.W. Cole, Phys. Rev. B **21**, 3713–3720 (1980)
19. M.W. Cole, D.R. Frankl, D.L. Goodstein, Rev. Mod. Phys. **53**, 199–210 (1981)
20. R.S. Berry, S.A. Rice, J. Ross, *Physical chemistry* (John Wiley, New York, 1980). Table 21.13
21. G. Stan, M.J. Bojan, S. Curtarolo, S.M. Gatica, M.W. Cole, Phys. Rev. B **62**, 2173–2180 (2000)
22. H. Margenau, N.R. Kestner, *Theory of intermolecular forces* (Pergamon, Oxford, 1969)
23. L.W. Bruch, M.W. Cole, H.-Y. Kim, J. Phys.: Condens. Matter **22**, 304001 (2010)
24. J.C. Phillips, *Covalent bonding in crystals and molecules and polymers* (University of Chicago Press, Chicago, 1969)
25. R. Langlet, M. Arab, F. Picaud, M. Devel, C. Girardet, J. Chem. Phys. **121**, 9655–9665 (2004)
26. L. Jensen, P.-O. Astrand, K.V. Mikkelsen, J. Phys. Chem. A **108**, 8795–8800 (2004)
27. L.X. Benedict, S.G. Louie, M.L. Cohen, Phys. Rev. B **52**, 8541–8549 (1995)
28. E.N. Brothers, A.F. Izmaylov, G.E. Scuseria, K.N. Kudin, J. Phys. Chem. **112**, 1396–1400 (2008)
29. K.S. Novoselov, A.K. Geim, S.V. Morozov, D. Jiang, M.I. Katsnelson, I.V. Grigorieva, S.V. Dubonos, A.A. Firsov, Nature **438**, 197–200 (2005)
30. J.C. Meyer, A.K. Geim, M.I. Katsnelson, K.S. Novoselov, T.J. Booth, S. Roth, Nature **446**, 60–63 (2007)
31. W.A. Steele, *Interaction of gases with solid surfaces* (Pergamon Press, New York, 1974)
32. W.A. Steele, Surf. Sci. **36**, 317–352 (1973)
33. B. Yakobson, R. Smalley, Am. Sci. **85**, 324–337 (1997)
34. E.N. Shamina, N.G. Lebedev, Russian. J. Phys. Chem. B **6**, 448–454 (2012)
35. L. Mandeltort, D.-L. Chen, W.A. Saidi, J.K. Johnson, M.W. Cole, J.T. Yates Jr, J. Am. Chem. Soc. **135**, 7768–7776 (2013). doi:10.1021/ja402928s